



HAL
open science

An accurate optical technique for measuring the nuclear polarisation of ^3He gas

Cavin Talbot, Marion Batz, Pierre-Jean Nacher, Geneviève Tastevin

► **To cite this version:**

Cavin Talbot, Marion Batz, Pierre-Jean Nacher, Geneviève Tastevin. An accurate optical technique for measuring the nuclear polarisation of ^3He gas. JCNS Workshop on Modern Trends in Production and Applications of Polarized ^3He , Jul 2010, Ismaning, Germany. pp.012008, 10.1088/1742-6596/294/1/012008 . hal-00562616

HAL Id: hal-00562616

<https://hal.science/hal-00562616v1>

Submitted on 3 Feb 2011

HAL is a multi-disciplinary open access archive for the deposit and dissemination of scientific research documents, whether they are published or not. The documents may come from teaching and research institutions in France or abroad, or from public or private research centers.

L'archive ouverte pluridisciplinaire **HAL**, est destinée au dépôt et à la diffusion de documents scientifiques de niveau recherche, publiés ou non, émanant des établissements d'enseignement et de recherche français ou étrangers, des laboratoires publics ou privés.

An accurate optical technique for measuring the nuclear polarisation of ^3He gas

Cavin Talbot¹, Marion Batz^{1,2}, Pierre-Jean Nacher¹, and Geneviève Tastevin¹

Abstract. In the metastability exchange optical pumping cells of our on-site production unit and of our other experimental set-ups, we use a light absorption technique to measure the ^3He nuclear polarisation. It involves weak probe beams at 1083 nm, that are either perpendicular or parallel to the magnetic field and cell axis, with suitable light polarisations. When metastability exchange collisions control the populations of the sublevels in the 2^3S state, absolute values of the ^3He ground state nuclear polarisation are directly inferred from the ratio of the absorption rates measured for these probe beams. Our report focuses on the transverse detection scheme for which this ratio, measured at low magnetic field for σ and π light polarisations, hardly depends on gas pressure or the presence of an intense pump beam. This technique has been systematically tested both in pure ^3He and isotopic mixtures and it is routinely used for accurate control of the optical pumping efficiency as well as for calibration of the NMR system.

¹ Laboratoire Kastler Brossel, ENS; CNRS; UPMC; 24 rue Lhomond, F-75005 Paris, France.

² Johannes Gutenberg University, Staudingerweg 7, D-55128 Mainz, Germany.

E-mail: nacher@lkb.ens.fr

1. Introduction

Metastability exchange optical pumping (MEOP) allows the polarisation of ^3He nuclear spins in pure helium gas and this technique is successfully used for production of highly polarised ^3He with large throughput. MEOP requires the electronic excitation of a small fraction of the He atoms to the metastable (2^3S) state and involves two co-operative processes: strong selective excitation on the 2^3S – 2^3P optical transition line at 1083 nm with transfer of angular momentum from polarised light to metastable He atoms; metastability exchange collisions with, for ^3He , transfer of nuclear polarisation from the metastable state to the ground state [1]. In pure ^3He gas, the driven radiative transitions enforce simultaneous orientation of the electronic and nuclear spins in the 2^3S state, entangled by the hyperfine interaction. In isotopic gas mixtures, radiative excitation can selectively enforce orientation of ^4He electronic spin in the metastable state but 2^3S polarisation builds up also for the ^3He isotope through metastability exchange between ground state ^3He and optically pumped ^4He atoms. For a detailed description of the MEOP process, we refer the reader to the companion contribution on MEOP basics in the same conference proceedings [1] as well as to comprehensive regular articles [2, 3, 4].

Radiofrequency (rf) discharges are frequently used for electronic excitation of a small (ppm) fraction of He atoms to the metastable state and MEOP performs better at low or moderate pressures (typically 0.5–5 mbar for operation at mT field strengths and 5–250 mbar for operation between 0.4 T and 4.7 T). Gas production units thus typically include a combination of several systems for high-purity gas handling, high-power optical pumping,

polarisation preserving compression, and long-term or short-term storage for massive centralised production or flexible on-site production, respectively. Diagnostic systems are also implemented for monitoring of the operating conditions and optimisation of the performances of the gas production units. NMR or magnetometry can be used to measure polarisation in the storage cell where large magnetisation is accumulated. In the optical pumping cell, optical methods such as polarimetry of the visible fluorescence light emitted by the plasma [5, 6, 7] or 1083 nm light absorption measurements [2, 4, 8, 9] are preferred because they provide much higher sensitivity and operate in the presence of the rf discharge.

All these techniques require calibration for accurate polarisation measurements, except the light absorption technique. The latter has actually been used for calibration purposes in the past decades [10, 11]. In contrast with the visible light polarimetry technique, that becomes inefficient above approximately 10 mT due to strong hyperfine decoupling in the highly excited energy levels involved in the radiative cascade, the absorption technique potentially operates at all field strengths [4]. It has been successfully used for high field MEOP investigations [4, 12, 13]. At low magnetic fields, recent work [14] has motivated more quantitative investigations of its potential artefacts in the context of very high power optical pumping.

In this contribution, we describe an accurate way to measure the ^3He nuclear polarisation at low magnetic field with the absorption technique, in various MEOP conditions. We report on systematic dedicated tests performed in small sealed He cells filled with pure ^3He gas or isotopic gas mixtures, we address the practical aspects of the experimental implementation, and quantitatively discuss the most relevant identified sources of errors in polarisation measurements.

2. Polarisation measurements with the light absorption technique

The absorption technique is based on the very strong link between the ground state nuclear polarisation M and the distribution of populations between the three (for ^4He) and six (for ^3He) Zeeman sublevels in the metastable state that is established by the frequent exchange collisions between the 2^3S atoms and the much more numerous ground state atoms. When metastability exchange dominates, a spin temperature distribution is enforced and the populations of the 2^3S sublevels scale exponentially with their respective angular momentum with a Boltzmann parameter $e^\beta = (1 + M)/(1 - M)$ [4]. The polarisation M can then be simply inferred from the ratio of populations in two 2^3S sublevels with distinct angular momenta for either isotope, or from independent linear combinations of such populations.

At low magnetic field, the 2^3S Zeeman sublevels are almost degenerate and two absorption measurements can be simultaneously performed with a monochromatic light source using different light polarisations. Three $2^3\text{S}-2^3\text{P}_0$ lines are well resolved in a low-pressure gas: the C_8 line ($2^3\text{S}, F=1/2-2^3\text{P}_0$) and the C_9 line ($2^3\text{S}, F=3/2-2^3\text{P}_0$) in pure ^3He , and the ^4He D_0 line ($2^3\text{S}-2^3\text{P}_0$) in isotopic mixtures. Picking up one of these lines, one may choose among the following simple schemes:

1/ *Transverse probe*: a weak laser beam propagates perpendicular to the axis of the magnetic field B and transmitted powers are measured for the orthogonal linear polarisations π (parallel to B) and σ (perpendicular to B). M is inferred from the ratio $r_\perp = A_\pi/A_\sigma$ of the corresponding absorption signals (see Section 3.5) A_π and A_σ , respectively. At zero magnetic field, the ground state ^3He nuclear polarisation is given by:

$$M = \pm \sqrt{\frac{1 - r_\perp^9}{1 + 2r_\perp^9}} \quad \text{for } \text{C}_9, \quad (1)$$

$$M = \pm \sqrt{\frac{1 - r_\perp^0}{1 + r_\perp^0}} \quad \text{for } \text{D}_0. \quad (2)$$

These formulas provide good approximations at small B if the probe is tuned to the centre of the absorption Doppler profile. For example, errors in M are lower than 2.5×10^{-3} for $|M| > 0.1$ and $B=1$ mT. For higher magnetic fields, they can still be used provided that r_{\perp} is replaced by the normalised ratio $R_{\perp}=r_{\perp}(M)/r_{\perp}(0)$ obtained by scaling r_{\perp} to its value at null polarisation, $r_{\perp}(0)$. If the probe laser is not tuned to the centre of the null-field or null-polarisation absorption profile, the detuning introduces a field-dependent error on $|M|$ of order $-0.02/\text{GHz/mT}$.

Polarisation cannot be measured with probe light tuned to C_8 because this line addresses the same pair of 2^3S sublevels ($F=1/2$, $m_F=\pm 1/2$) for π and σ polarisations, hence the ratio r_{\perp}^8 does not depend on M . The C_9 line cannot be used for polarisation measurements in mixture cells because it overlaps with the strong unresolved D_1 and D_2 lines ($2^3\text{S}-2^3\text{P}_1$ and $2^3\text{S}-2^3\text{P}_2$, respectively) of the ^4He isotope. Therefore, absorption measurements are performed with the probe laser tuned to the C_9 line in pure ^3He gas and to the D_0 line in isotopic mixtures.

2/ Longitudinal probe: the weak laser beam propagates parallel to B , transmitted powers are measured for the two circular polarisations σ_+ and σ_- , and M is inferred from the ratio $r_{\parallel}=A_{\sigma_+}/A_{\sigma_-}$ of the absorption signals A_{σ_+} and A_{σ_-} , respectively. At zero magnetic field, the ground state ^3He nuclear polarisation is given by:

$$M = \frac{1 - r_{\parallel}^8}{1 + r_{\parallel}^8} \quad \text{for } \text{C}_8, \quad (3)$$

$$M = \frac{1 - \sqrt{r_{\parallel}^0}}{1 + \sqrt{r_{\parallel}^0}} \quad \text{for } \text{D}_0. \quad (4)$$

The polarisation components σ_+ and σ_- individually address a single sublevel for these two single-component lines ($m_F=-1/2$ and $+1/2$, respectively, for C_8 and $m_J=-1$ and $+1$, respectively, for D_0) and the ratio r_{\parallel} directly measures at $B=0$ the ratio of populations in the probed Zeeman sublevels. As is done for the transverse probe, r_{\parallel} can be replaced by the normalised ratio $R_{\parallel}=r_{\parallel}(M)/r_{\parallel}(0)$ in formulas (3) and (4) to obtain accurate results in an applied field. Moreover, the use of reduced ratios also eliminates the error introduced by probe detuning for the longitudinal probe scheme.

No simple analytical formula exists for the C_9 line for which each polarisation component addresses simultaneously two Zeeman sublevels. Instead, the relation:

$$r_{\parallel}^9 = \left(\frac{2 - M}{2 + M} \right) \left(\frac{1 - M}{1 + M} \right)^2 \quad (5)$$

has to be solved (e.g., finding the root of a cubic polynomial, numerically, or using polynomial fits...) to infer M from r_{\parallel}^9 .

Figure 1 shows the variations of r_{\perp} and r_{\parallel} with M . For the transverse probe scheme, C_9 and D_0 lines provide a comparable sensitivity for polarisation measurements, quite high above $|M| \geq 0.2$. The sensitivity is reduced at small M , with a quadratic departure of r_{\perp} from 1 that results from the fact that each light component simultaneously addresses sublevels with opposite angular momenta. In contrast, the longitudinal probe scheme has a linear response at small M for all lines, with a higher sensitivity for the C_9 and D_0 lines. At high M , it has a reduced sensitivity for C_9 and D_0 with $r_{\parallel} \propto (1 - M)^2$; the C_8 line retains a linear sensitivity, yet provides a limited precision since both absorption signals vanish at $M=1$.

During optical pumping, a strong pump beam tends to enforce a distribution of populations in the 2^3S states that departs from the spin-temperature distribution that would result from metastability exchange only. The above equations then provide apparent polarisations M^{app} that depend on the choice of detection scheme and probe line and differ from the actual nuclear polarisation M . Examples of experimental deviations of M^{app} from M are discussed in Section 5.

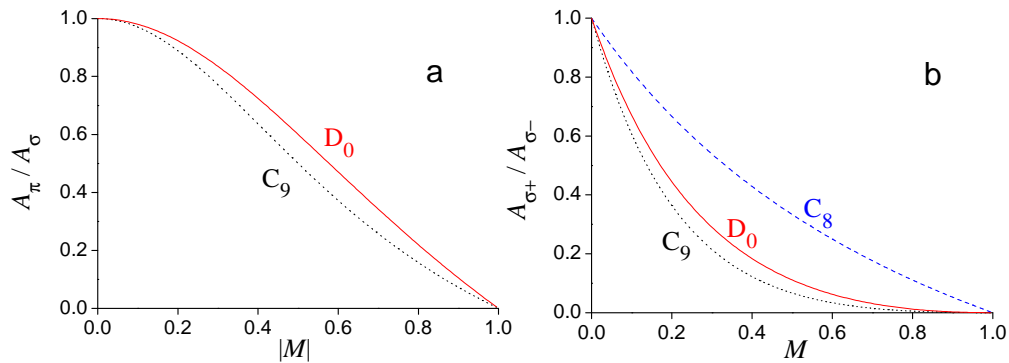


Figure 1. Ratios of $2^3\text{S}-2^3\text{P}_0$ absorption signals computed for the transverse (a) and longitudinal (b) probe schemes as a function of ground state nuclear polarisation M , at zero magnetic field and at spin temperature equilibrium. **a-** Transverse probe scheme: D_0 (solid line) and C_9 (dotted line) provide comparable sensitivities at all M . Opposite polarisations M and $-M$ cannot be distinguished using A_π/A_σ . **b-** Longitudinal probe scheme: C_9 (dotted line) and D_0 (solid line) provide higher sensitivity than C_8 (dashed line) at small M , where accurate measurements can be performed in contrast with the transverse scheme. Identical curves would be obtained by plotting the inverted ratio $A_{\sigma^-}/A_{\sigma^+}$ for negative M values.

3. Experimental apparatus

3.1. Probe laser

The probe laser consists of a linearly polarised 70 mW DFB laser diode (Toptica Photonics AG) housed within a temperature-regulated aluminium box for wavelength stability. Inside this box the divergent elliptical beam from the laser diode is collimated and then reshaped to circular with a pair of anamorphic prisms. The beam passes through a Faraday isolator before being coupled into a polarisation preserving monomode optical fibre as it exits the aluminium box. The laser can thus be situated remotely to the helium polarising equipment for both convenience and reduced impact on the magnetic field map. Typically 15 milliwatts are coupled into the fibre when the laser diode is running at maximum current. Laser stability and control are achieved with an in-house electronic controller. The aluminium box is heated to a fixed set point above room temperature with a resistive element for long term thermal stability and the laser frequency is adjusted using the on-chip thermoelectric cooler.

3.2. Probe assembly for the transverse probe scheme

Figure 2 shows a schematic diagram of the probe assembly and its caption includes all technical details. The laser diode light that exits the optical fibre tip is collimated and split in two adjacent beams with σ and π polarisations. This is in contrast with prior implementation [10], in which probe beams spatially overlapped. The beam separation preserves the accuracy of the polarisation measurements for all probe tunings, as discussed in Section 5.1. The beams propagate across the helium cell, entering and exiting through the curved glass walls. A cylindrical lens is used to correct for the resulting wavefront distortions before back-reflection through the lens and cell. One of the beams is then deflected by a polarising beam splitter (PBS) cube. Both beams are coupled by lenses into 1-mm core multimode plastic fibres that are connected to the photodiodes. The photodiode voltages are recorded on a PC using a USB data logger for post processing.

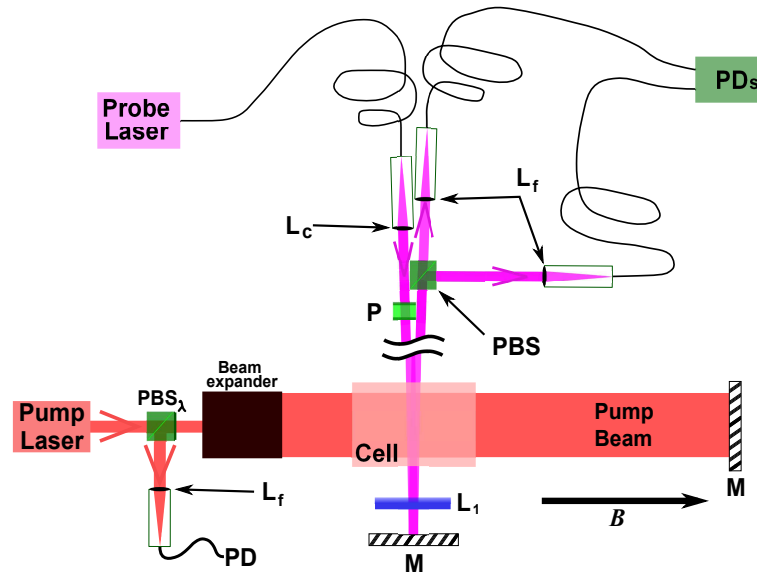


Figure 2. Schematic of the transverse probe assembly. Optical elements include: mirrors (M), photodiodes (PD); a collimating lens (L_c , $f=40\text{mm}$), a polarising cube (PBS), and a compensating cylindrical lens (L_1 , $f=500\text{mm}$), and collecting lenses (L_f , $f=30\text{mm}$) on the probe path; a circular polariser (PBS_λ , a PBS cube with glued quarter wave plate) and a collecting lens (L_f , $f=30\text{mm}$) on the pump path. The collimated laser diode probe beam is split in two halves by P, a pair of co-planar polarising plates with crossed linear axes attached to a mask that consists in a 8 mm circular hole with a central 1.5-mm broad beam stopper. The exiting collinear beams with polarisations π (along B) and σ (perpendicular to B) cross the cell at almost normal incidence (2° tilt). The distance between cell axis and probe beam collection is approximately 50 cm.

3.3. Pump laser

For optical pumping a 5 Watt broadband (1.7 GHz fwhm) 1083 nm fibre laser is used (Keopsys, model YFL-1083-50-COL). The collimated Gaussian output beam is circularly polarised and expanded to a diameter of 2 cm fwhm. It propagates along the direction of the magnetic field and passes twice through the cell. The transmitted light, deflected by the circular polariser, is monitored by a photodiode for checks of the laser tuning and measurements of the pump power absorption.

3.4. Helium test cells

The sealed helium cells used for these investigations are pyrex glass tubes with flat end windows (5 cm in diameter 5 cm long). They contain ^3He at various gas pressures, either pure or mixed with set ratios of ^4He . However some of the “pure ^3He ” cells actually contain traces of ^4He plausibly left from the cleaning process prior to the filling of the cells.¹ A discharge is generated in the cell using two external wire electrodes connected to a tuned voltage transformer fed by a rf generator able to produce 5 W in the 1 to 3 MHz range. This rf excitation is amplitude modulated at around 70 Hz and lock-in detection is used to improve sensitivity of the absorption measurements.

¹ ^4He concentrations, measured by comparison of absorption rates on the resolved C_s and D_0 isotopic lines, range from 0.1 to 2 %.

3.5. Absorption signals

The absorption signals A_π and A_σ used for nuclear polarisation measurement are the amplitudes of the modulation depth (i.e., the ratios of the ac amplitudes to the dc components) of the corresponding probe powers exiting the cell. Each ratio is robust against fluctuations of the incident power I_0 and directly proportional to the absorbance $-\ln(I/I_0)$, with a coefficient that only depends on the plasma response to the rf excitation [4, 15]. For improved accuracy, the PBS cube (transmission efficiency: $1-\epsilon=0.96$) is oriented so as to transmit the π component for which the absorbance is very small at high nuclear polarisation ($A_\pi \rightarrow 0$ for $M \rightarrow 1$) and to deflect the σ component. In this configuration, the amplitudes S_π and S_σ of the modulation depth of the photodiode voltages are related to the absorption signals by $S_\pi=(1-\epsilon)A_\pi$ and $S_\sigma=A_\sigma+\epsilon A_\pi$. This is used to compute the ratio r_\perp of absorption signals from processed photodiode voltage data:

$$r_\perp = A_\pi/A_\sigma = \frac{S_\pi}{S_\sigma - \epsilon S_\pi/(1 - \epsilon)}. \quad (6)$$

3.6. NMR detection

For comparison with optical measurement results, NMR measurements have been performed at 28 kHz (the Larmor precession frequency for $B=0.87$ mT) using a homebuilt NMR detection system that consists of crossed induction and detection coils set around the test cell. Since the gas density is low, 90° tipping pulses are routinely used to obtain good signal-to-noise ratios (typically up to 100), with tens of seconds of precession lifetimes T_2 . NMR signals are proportional to the fixed number N_3 of ^3He atoms contained in the glass cell and to the nuclear polarisation M . They have to be scaled for cell content and volume for direct comparison to the nuclear polarisations measured using the absorption technique.

The gas pressures slightly differ from the filling pressures for the sealed cells that are several decades old and the actual pressures are measured by NMR. For each cell, the decay rates of free precession signals, $1/T_2$, have been measured for various applied magnetic field gradients to obtain the ^3He diffusion coefficient D [16]. D is inversely proportional to gas pressure P for pure ^3He gas ($D=1.997 \times [T/300]^{1.71}/P$, with temperature T in K and P in atm) and depends on the partial pressures of ^3He and ^4He gas for isotopic mixtures (see reference [17], and corrected values of diffusion coefficients in [18]).

4. Polarisation measurements

Figure 3 shows probe recordings and processed data from a typical polarisation experiment. During the acquisition, the photodiode voltages and TTL reference signal are continuously recorded. Figure 3a shows a small section of the recorded transmitted probe powers in which the modulation of the absorption is clearly seen. Initially (part C) the gas is not polarised ($M=0$) and the modulation depth of the π and σ components are equal; later (part D) the gas is polarised ($M=0.5$) and both absorption rates and modulation depths are different for the two components. Figure 3b shows the time evolution of the average absorption signals and computed nuclear polarisation during the entire experiment. The plot is divided into six regions that are related to the six main steps of the acquisition protocol, as follows:

- (A) the laser beams are blocked and the rf discharge is off; offset voltages are recorded.
- (B) the probe block is removed and discharge is off; incident probe powers I_0 are measured.
- (C) the rf discharge is on; transmitted probe powers I are measured at null polarisation.
- (D) the pump block is removed; optical pumping takes place and polarisation increases.
- (E) the pump beam is blocked again when polarisation is close to steady-state; polarisation decreases due to plasma-induced decay for some arbitrary time period.
- (F) the rf discharge is turned off; NMR signal is acquired to measure the magnetisation associated with the remaining polarisation M .

Nuclear polarisation is fully destroyed in the cell by the 90° rf pulse used for the NMR measurement. MEOP is performed to repolarise the gas and another measurement can be made for a different polarisation M after a shorter or longer decay period.

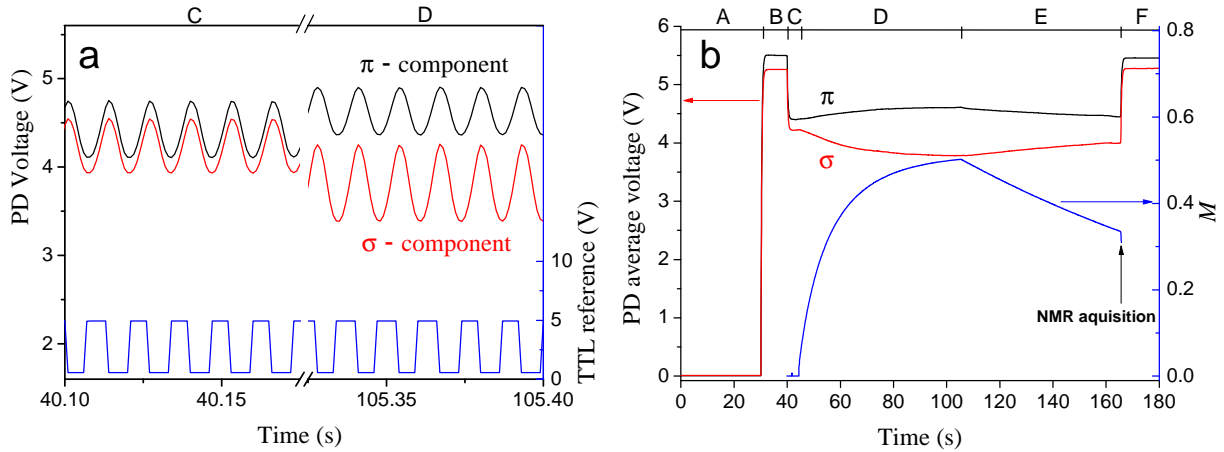


Figure 3. Example of raw and processed data from a typical polarisation experiment performed on the 1.3 mbar cell. The probe laser is tuned to the C_9 transition with 0.14 mW of output power. The polarisation is achieved by MEOP using the pump laser tuned to C_8 with 2.5 W of output power. Fig. 3a shows two subsections of the raw voltage recordings (upper traces: PD voltages, lower trace: TTL reference signal). Section C: discharge is on, pump is blocked, and transmitted probe powers are recorded at $M=0$, showing equal modulation depths ($\sim 10\%$). End of section D: after 60 s of MEOP, the ratio of the modulated absorptions is significantly modified. Fig 3b shows the time averaged probe signals (upper traces) and the computed M (lower trace) for an entire polarisation experiment. The signal-to-noise ratio exceeds 3000 at $M=0.5$ for an averaging time constant of 0.3 s.

Excellent linear correlation is obtained between the two independent sets of polarisation measurements (NMR and optical probe). In all the pure ^3He cells the absorption technique is checked to yield data that consistently agree with the NMR data scaled to actual gas pressures. In the mixture cells, the absorption technique using the D_0 line yields data that also fully agree with the NMR data scaled to ^3He partial gas pressures. This agreement confirms that the nuclear polarisation of ground state ^3He atoms imposes a spin temperature distribution in the ^4He metastable state as well.

5. Discussion

5.1. Implementation and design

The absorption measurements are performed on the same infrared transition as the optical pumping. Contribution to the measured transmitted powers from the 1083 nm fluorescence light emitted by the gas subjected to intense pumping should thus be limited, as usual, by reducing the detected solid angle to a minimum. Alternatively, when fluorescence light and stray light from the intense pump laser cannot be avoided, a double modulation scheme (e.g., with a probe frequency swing in and out resonance or mechanical beam chopping) may help. The stray light contribution is a minor issue for the transverse probe scheme, when compared to the longitudinal one. However the absorbed probe power (hence the signal-to-noise ratio) is generally lower with transverse probe scheme, especially in the long cells used for gas production.

In order to measure absolute ratios of populations, the two probe components should ideally overlap exactly. However, in this situation, polarisation components reaching the same 2^3S Zeeman sublevel may interact. The scaled ratio of absorption signals $R_{\perp} = r_{\perp}(M)/r_{\perp}(0)$ has been observed to exhibit small frequency-dependent variations at finite nuclear polarisations, both when the probe is tuned to the C_9 line in ^3He gas and when it is tuned to the D_0 line in isotopic gas mixtures. Similar observations have been made with the longitudinal probe scheme for $R_{\parallel} = r_{\parallel}(M)/r_{\parallel}(0)$ in pure ^3He gas when absorption measurements are performed on the C_9 line, but no such artefact has been noticed when the C_8 line is used. Systematic investigations have been made for both probe schemes in a variety of experimental conditions and detailed results will be reported elsewhere. Using two separate beams for the absorption measurements, as described in Section 3.2 for the transverse probe scheme, has been checked to make the optical technique robust against probe detuning and accurate at all polarisations (for both probe schemes). These probe beams still remain very close so as to address nearly identical sets of atoms, and any small local differences (e.g., in the number density of metastable atoms) cancel out when reduced ratios R_{\perp} or R_{\parallel} are used.

5.2. Impact of the probe light intensity

The light intensity in the probe beam must be low enough so as not to induce significant distortion of the 2^3S population distribution in the metastable state [4]. This distortion may be expected to scale as γ_p/γ_e in pure ^3He gas, where γ_e is the metastability exchange rate and γ_p is the relevant average optical pumping rate for the probed line components. γ_e is proportional to gas pressure P ($\gamma_e=3.75\times 10^6\text{ s}^{-1}/\text{mbar}$ for ^3He [19]) and γ_p is proportional to the light intensity and scales as $1/P$, due to the impact of velocity-changing collisions on the fraction of the atomic Doppler profile actually addressed by the single-frequency probe light [3]. We have performed checks of this effect by measuring the ratios r_{\perp}^9 and r_{\perp}^0 for $M=0$ in two ^3He cells and in a mixture cell, respectively. They decreased linearly with decreasing probe intensity, with slopes consistent with expectations and obeying the $1/P^2$ scaling for pure ^3He .

The light intensity should be reduced until it does not affect the measurements. For instance, for a probe intensity of $100\text{ }\mu\text{W}/\text{cm}^2$, M is overestimated at low pressure ($P=0.43\text{ mbar}$) by as much as 0.05 for $M=0$ and 0.01 for $M=0.1$. These errors are reduced to 0.023 ($M=0$) and 0.002 ($M=0.1$) for a probe intensity of $25\text{ }\mu\text{W}/\text{cm}^2$. It is possible to keep the intensity of the probe low by reducing the incident power and/or increasing the beam diameter. The second option is usually preferred because it preserves the signal-to-noise ratio. These limits on probe intensity are significantly less stringent if a broadband laser is used, such as the monitor output of the fibre laser used for optical pumping. The actual distortion of population distribution is then reduced by the ratio of linewidth (of order 100) at given laser intensity, hence intensities of order $1\text{ mW}/\text{cm}^2$ may be used.

5.3. Impact of the probe light power

The probe-driven optical pumping cycles may also influence the time evolution of nuclear polarisation because they contribute to the overall angular momentum budget [1]. No angular momentum is associated to the π and σ components of the transverse probe but, since the probe light equally addresses sublevels with opposite angular momenta, it tends to more efficiently depopulate the overpopulated ones. As a result it drives the 2^3S state towards a null average nuclear orientation and, through metastability exchange, contributes to the ^3He polarisation decay in the ground state. This may limit the MEOP performances in optical pumping experiments, in a way that is similar to what occurs for an imperfectly polarised pump beam. This may also influence the evolution of the polarisation in the absence of pump light and introduce a noticeable additional decay rate. The additional decay rate is expected to scale with the absorbed power (hence, with the 2^3S number density) and to be inversely

proportional to the number of ground state atoms (hence, to the ^3He gas partial pressure and to the cell volume). This has been experimental checked by recording polarisation decays in the plasma for various probe beam powers. Figure 4 shows that decay rates increase linearly

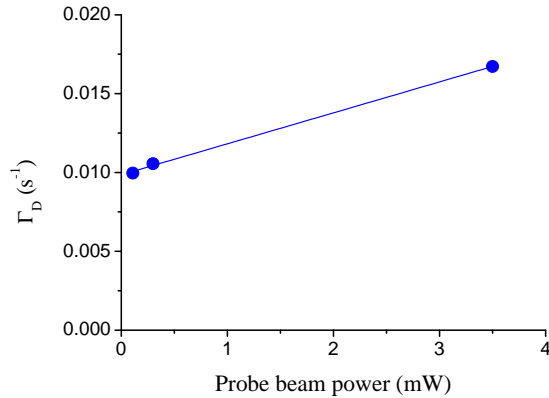


Figure 4. Examples of polarisation decay rates plotted as a function of probe power in the transverse probe scheme. The slope indicates a probe-induced additional decay rate of $2 \times 10^{-3} \text{ s}^{-1}/\text{mW}$, consistent with expectations for these experiments (0.43 mbar cell, 9% probe absorption).

with probe powers at fixed rf discharge excitation, as expected. Depending on the objective of the polarisation measurement, a trade-off between a high signal-to-noise ratio and a negligibly small action of the probe has to be found; probe powers in the range 0.1-1 mW are usually a safe choice. When long cells are used, the increase in their volume proportionally decreases the impact of probe power, but in the transverse scheme only.

5.4. Impact of the pump light

The deviation from spin temperature distribution of populations induced by the strong pump light, that provides the driving term for the build up of the ground state ^3He polarisation, results in modified absorption rates for the two probe beams [1]. The apparent polarisation values M^{app} obtained using the relevant spin temperature formula (Eqs. (1) to (5), depending on the detection scheme) overestimate the actual polarisations M and the pump-induced differences $M^{\text{app}} - M$ can be experimentally measured when the pump is rapidly applied or blocked, at steady-state or at arbitrary M during polarisation build-up. Results of dedicated experiments performed to quantify this difference for both probe schemes in similar OP conditions are shown in Figs. 5 and 6.

Data points in Fig. 5 have been individually obtained using the protocol described in Section 4 for various polarisation growth times. The uncertainties mainly result from polarisation changes during the time required to manually block the OP beam. The pump-induced differences decrease when gas pressure rises (from 0.43 to 5.4 mbar), due to the increased metastability exchange rate that competes with optical pumping for population distribution, and steadily decrease with high nuclear polarisations at all pressures. When the same line is used for OP and for detection, the pump and probe beams address the same 2^3S Zeeman sublevels and the pump-induced differences are observed to be about twice as large as in Fig. 5 (data not shown).

Each of the four data sets in Fig. 6 has been obtained from a single recording, where short periods of polarisation build-up alternated with periods with a blocked pump. For each choice of probe line, the pump-induced differences systematically decrease again with pressure and polarisation, and they increase by a factor of five when the C_8 line is used instead of the C_9 line for the probe. When the C_9 line is used for pumping (data not shown), the pump-induced differences for each pressure are similar for the two probe lines and about twice as large as those represented by the solid symbols in Fig. 6.

Comparison of Fig. 5 to Fig. 6 shows that the transverse probe scheme is significantly less prone to the impact of pump light than the longitudinal probe scheme (5 to 10 times less,

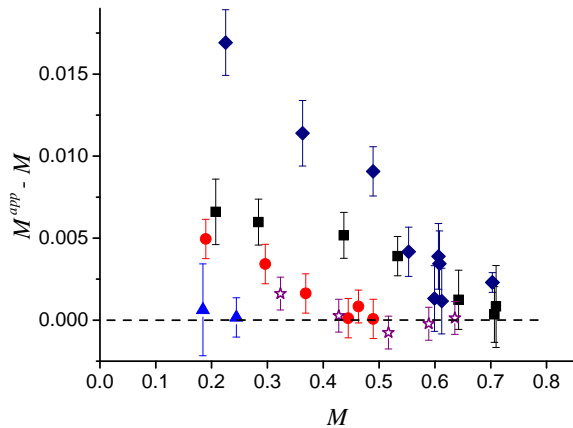


Figure 5. Measured pump-induced differences $M^{\text{app}}-M$ for the transverse probe scheme at various pressures and polarisations. OP is made with 1.5 W laser output power tuned to the C_8 line. Solid symbols: C_9 probe, pure ^3He gas, (diamonds: 0.43 mbar; squares: 1 mbar; circles: 1.33 mbar; triangles: 5.41 mbar). Open stars: D_0 probe, mixture cell (1 mbar ^3He and 0.47 mbar ^4He).

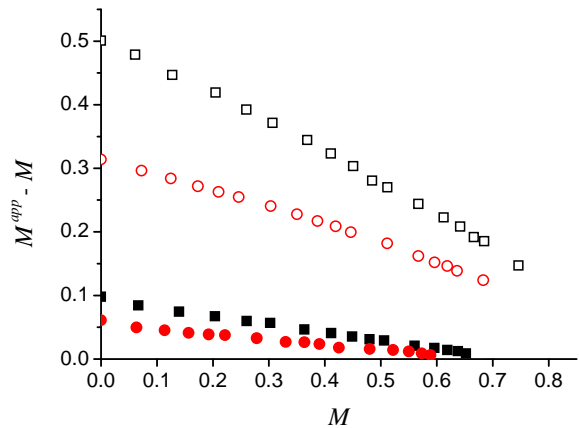


Figure 6. Measured pump-induced differences for the longitudinal probe scheme (note the difference in vertical scales with Fig. 5). OP is made with 2 W laser output power tuned to the C_8 line (beam diameter: 1.4 cm fwhm) in 6 cm diameter 30 cm long cells filled with pure ^3He gas (squares: 0.63 mbar; circles: 1.19 mbar). Solid symbols: C_9 probe; open symbols: C_8 probe. The schematic of the longitudinal probe assembly used for the measurements is given in [1].

depending on the chosen OP transition). This is due to partial compensation of the effects on the transverse absorption signals of the pump-driven depopulation and overpopulation for pairs of 2^3S sublevels with opposite angular momenta. For both detection schemes, pump-induced differences increase with laser power until optical saturation of the $2^3\text{S}-2^3\text{P}_0$ occurs (typically above $1\text{W}/\text{cm}^2$).

In previous work using a transverse probe scheme [10], accurate comparisons of the absorption and polarimetry techniques had been performed without pump light, during polarisation decay. The reported absence of noticeable difference between the polarisations measured with (M^{app}) and without (M) pump beam explicitly refers to comparisons performed at steady-state polarisations. It can be explained by the limited signal-to-noise ratio (Fig. 4 of [10]) obtained with the single-pass probe path and by the high nuclear polarisations achieved with a broadband 3W laser ($M \geq 0.5$).

For standard operating conditions, the nuclear polarisation exceeds 0.5 in the optical cells of our gas production unit and the steady-state pressure is on the order of 1.33 mbar. Overlooking the small difference between M^{app} and M results in an absolute error smaller than 0.25% and relative errors systematically lie below 0.5% when the transverse probe scheme is used.

5.5. Impact of ^4He impurities

Residual ^4He atoms may contribute to probe light absorption due to the overlap of the D_1 and D_2 lines with the C_9 line ^3He atoms. Computations performed for the upper bound of ^4He concentrations measured in the sealed test cells (2%) yield, for instance, $M^{\text{app}}=56\%$ for $M=60\%$. The relative error approximately scales with the ^4He concentration .

6. Conclusions

We have reported implementation and systematic tests of the transverse probe scheme for absolute polarisation measurements with the absorption technique. The consistency and high accuracy of the measurements have been demonstrated and assessed by correlation with NMR measurements as well as by comparison with numerical results obtained with a MEOP model. Potential systematic errors have been discussed and a number of simple experimental tests have been described to check that they actually remain well below the percent level.

Most experiments have been performed using a single-frequency laser diode to probe 2^3S - 2^3P_0 absorption. The technique can be applied also using a broadband light source. The overall decrease in probe light absorption has no influence on the computed M values, but data reduction becomes less straightforward as some contribution to light absorption comes from the wings of neighbouring resonance lines for very broad lasers. We have performed test measurements with the weak monitor beam provided by the supplementary output of the pump laser, but low accuracy has been obtained with this more noisy light source. Moreover, its use is restricted to situations where MEOP is performed using the C_9 or D_0 line.

The probe assembly that we have described has also been used for polarisation measurements in the long valved cell (50 cm length, 6 cm diameter) of our gas production unit to characterise the efficiency of MEOP in various operating conditions. For improved performance, a double cell with two such glass cylinders connected in series has been recently implemented in the unit. The same transverse probe assembly is currently used for simultaneous polarisation measurements in the two gas compartments. Successful measurements are performed with a configuration similar to that of Fig. 2 where the probe beam propagates successively through the two glass cells before back-reflection by the mirror. Using two different frequencies for the discharge modulation in each cell, their individual contributions to the absorption signal can be singled out by selective lock-in detection. In spite of the lower signal-to-noise ratios obtained with the transverse probe scheme, the simpler technical implementation makes this scheme quite advantageous over the longitudinal one for polarisation measurements in multiple cells with a single laser beam.

The transverse probe scheme provides a very robust way to perform absolute measurements of the ^3He nuclear polarisation in all situations where the gas pressure is not well known or variable in time. Gas production units operate either in batch mode (no gas flow) or in continuous mode (gas flow through the optical pumping cell where fresh gas gets polarised), in general with no easy and non-relaxing way to measure on-line the pressure inside the MEOP cell. The longitudinal probe scheme is more sensitive at low polarisations, but dedicated experiments must be performed to establish the pressure-dependent correspondence between M^{app} and M . The use of this scheme may be restricted to batch mode operation or to reproducible stationary conditions of gas flow. The transverse probe scheme is therefore the best suited one for accurate on-line polarisation measurements.

Acknowledgments

The authors wish to thank Raphaël Lambert for his contribution to an early stage of the work. This research program is supported in part by the European Commission (PHeLINet Marie Curie Research and Training Network grant).

References

- [1] Batz M, Nacher P J and Tastevin G 2011 Fundamentals of metastability exchange optical pumping in helium *Proceedings of this conference* ISSN 0000-0000
- [2] Colegrove F D, Schearer L D and Walters G K 1963 *Phys. Rev.* **132** 2561–2572
- [3] Nacher P and Leduc M 1985 *Journal de Physique* **46** 2057–2073 URL <http://dx.doi.org/10.1051/jphys:0198500460120205700>
- [4] Courtade E, Marion F, Nacher P J, Tastevin G, Kiersnowski K and Dohnalik T 2002 *The*

- European Physical Journal D - Atomic, Molecular, Optical and Plasma Physics* **21** 25–55 URL <http://dx.doi.org/10.1140/epjd/e2002-00176-1>
- [5] Laloë F 1971 *Ann. Phys. Fr.* **6** 5–& ISSN 0003-4169
- [6] Pavlovic M and Laloë F 1970 *J. Phys.* **31** 173–& ISSN 0302-0738
- [7] Stoltz E, Villard B, Meyerhoff M and Nacher P 1996 *Applied Physics B: Lasers and Optics* **63** 635–640 ISSN 0946-2171
- [8] Greenhow R C 1964 *Phys. Rev.* **136** A660–A662
- [9] Daniels J and Timsit R 1971 *Canadian Journal Of Physics* **49** 539 ISSN 0008-4204
- [10] Bigelow N P, Nacher P J and Leduc M 1992 *Journal de Physique II* **2** 2159–2179 ISSN 1155-4312 URL <http://dx.doi.org/10.1051/jp2:1992258>
- [11] Lorenzon W, Gentile T R, Gao H and McKeown R D 1993 *Phys. Rev. A* **47** 468–479
- [12] Abboud M, Sinatra A, Maitre X, Tastevin G and Nacher P J 2004 *EPL (Europhysics Letters)* **68** 480–486 URL <http://dx.doi.org/10.1209/epl/i2004-10237-y>
- [13] Suchanek K, Suchanek M, Nikiel A, Palasz T, Abboud M, Sinatra A, Nacher P J, Tastevin G, Olejniczak Z and Dohnalik T 2007 *European Physical Journal - Special Topics* **144** 67–74 ISSN 1951-6401
- [14] Batz M 2011 *Metastability exchange optical pumping of ^3He in magnetic fields up to 30 mT: Systematic investigations of performances and relaxation mechanisms* Ph.D. thesis UPMC - Paris 6 and Johannes Gutenberg-Universität Mainz
- [15] Courtade E 2001 *Pompage optique de l'hélium dans des conditions non-standard (See Appendix 1)* Ph.D. thesis Université Pierre et Marie Curie - Paris 6 URL <http://tel.archives-ouvertes.fr/tel-00001447>
- [16] Hayden M E, Archibald G, Gilbert K M and Lei C 2004 *Journal of Magnetic Resonance* **169** 313 – 322 ISSN 1090-7807 URL <http://www.sciencedirect.com/science/article/B6WJX-4CKNKRY-2/2/4a1f0a7681653c8805d13eb753b578b0>
- [17] Bidinosti C P, Choukeife J, Nacher P J and Tastevin G 2003 *J. Magn. Reson.* **162** 122 – 132
- [18] Tastevin G and Nacher P J 2005 *J. Chem. Phys.* **123** 064506 ISSN 0021-9606
- [19] Dupont-Roc J, Leduc M and Laloë F 1971 *Phys. Rev. Lett.* **27** 467–470